Comparative nanostructure analysis of gasoline turbocharged direct injection and diesel soot-in-oil with carbon black

S.A. Pfau [a], A. La Rocca [a, *], E. Haffner-Staton [a], G.A. Rance [b, c], M.W. Fay [a, b], R.J. Brough [a], S. Malizia [a]

[a] Department of Mechanical Materials and Manufacturing Engineering, University of Nottingham, UK
[b] Nanoscale and Microscale Research Centre, University of Nottingham, UK
[c] School of Chemistry, University of Nottingham, UK

ARTICLE INFO

ABSTRACT

Two gasoline turbocharged direct injection (GTDI) and two diesel soot-in-oil samples were compared with one flame-generated soot sample. High resolution transmission electron microscopy imaging was employed for the initial qualitative assessment of the soot morphology. Carbon black and diesel soot both exhibit core-shell structures, comprising an amorphous core surrounded by graphene layers; only diesel soot has particles with multiple cores. In addition to such particles, GTDI soot also exhibits entirely amorphous structures, of which some contain crystalline particles only a few nanometers in diameter. Subsequent quantification of the nanostructure by fringe analysis indicates differences between the samples in terms of length, tortuosity, and separation of the graphitic fringes. The shortest fringes are exhibited by the GTDI samples, whilst the diesel soot and carbon black fringes are 9.7% and 15.1% longer, respectively. Fringe tortuosity is similar across the internal combustion engine samples, but lower for the carbon black sample. In contrast, fringe separation varies continuously among the samples. Raman spectroscopy further confirms the observed differences. The GTDI soot samples contain the highest fraction of amorphous carbon and defective graphitic structures, followed by diesel soot and carbon black respectively. The $A_{D1}:A_G$ ratios correlate linearly with both the fringe length and fringe separation.

© 2018 The Authors. Published by Elsevier Ltd. This is an open access article under the CC BY license (http://creativecommons.org/licenses/by/4.0/).

1. Introduction

Due to increasingly stricter emission regulations, automotive companies strive for new ways to optimize internal combustion engines. As such, direct injection systems offer significant improvements for gasoline engines in terms of fuel efficiency and CO_2 emissions [1]. Combining such technology with turbochargers, engine downsizing becomes feasible and enables further performance enhancements [2,3]. However, gasoline turbocharged direct injection (GTDI) engines exhibit higher particulate matter (PM) emissions than port fuel injection (PFI) engines. While the issue of PM emissions has been thoroughly investigated for diesel engines, to date there has been comparitively little research on GTDI engines.

Generally, the formation of particulate matter or soot occurs in the combustion chamber under fuel rich conditions [4,5]. If the fuel

is directly injected, the time before ignition is not sufficient for the fuel to mix completely with the compressed air. Combustion of localized areas of the non-stoichiometric mixture leads to the formation of small unsaturated and radical species, of which acetylene is generally considered to be the most important precursor to soot formation [6]. Polymerization reactions between these initial species lead first to the formation of small aromatic molecules, and continue forming extended polyaromatic species known as polyaromatic hydrocarbons (PAH). Further growth of these large molecular species leads directly to the inception of particle phase soot species of around 2000 u (unified atomic mass unit) at ca. 1.5 nm in diameter [6]. These particles continue to grow in size and mass due to the addition of vapour phase species to their surface and coagulation of particles due to their collision forming spherical 'primary particles' typically 10–50 nm in diameter [7]. Further agglomeration of these primary particles forms the characteristic fractal soot nanoparticles. Oxidation is pervasive throughout the soot formation process due to the highly oxidizing conditions within the cylinder, and acts to reduce the size and number of the soot

nanoparticles produced. Both the formation and oxidation are highly dependent on the engine operating conditions, such as injection modes [8,9], cold start conditions [10,11] or engine speed and load [10,12,13].

While the majority of PM leaves the cylinder with the exhaust gas, a small fraction of the particles transfer into the lubricating oil via a thermophoretic mechanism following impingement on the combustion chamber walls or via blow-by gases [14]. The implications of diesel soot particles on wear of the engine have been investigated by various researchers. Gautam et al. [15] found that the wear of lubricated engine components is proportional to the soot concentration in the lubricating oil. Studies by Sato et al. [16] and Green et al. [14] confirmed this observation and discovered further that the effect is more significant for thinner films, e.g. in the valve train. As such, the camshaft undergoes wear in the form of surface degradation and reduction in cam diameter, resulting in increases in friction and impeded cylinder gas exchange due to reduced valve amplitudes respectively. Consequently, the engine efficiency is reduced.

Antusch et al. [17] established that the wear rate not only depends on the concentration of soot, but also on the interaction of soot particles with oil additives, i.e. the chemical properties, morphology, and reactivity of the particles. While diesel soot was found to be more structured and to promote a logarithmic increase in wear rate with run time, GTDI soot appeared more amorphous and caused a constant increase in wear rate with run time. A higher degree of disorder in the GTDI soot leaves more reactive sites on its surface, thus allowing for more interactions with the lubricating oil compared to diesel soot. In contrast, Uy et al. [18] observed similarities in the morphology between diesel and GTDI soot samples. However, the latter exhibited higher concentrations of wear metals and oil additives, as well as some regions with a sludge-like structure. Barone et al. [19], as well as Gaddam and Vander Wal [20] also identified similarities in the nanostructure of GTDI and diesel soots, although larger primary particles were seen for GTDI. A subsequent study by Liati et al. [21] found GDI soot nanostructure to be less ordered than diesel soot, indicating that the former may contain organic compounds that prevent crystallisation. The disorder and curvature of the graphene layers in the shell of soot nanoparticles has also been linked to differences in oxidative reactivity, as shown by Vander Wal and Tomasek [22] as well as Alfè et al. [23]. Furthermore, the nanostructure can impede the effectiveness of oil additives, such as dispersants, as established by Esangbedo et al. [24].

Reactivity of soot is a consequence of both agglomerate morphology and the nanostructure and chemical composition of primary particles. It is not only an important facet of soot characterisation in relation to its entrainment within oil films, but it is directly related to many other undesirable effects caused when a variety of environments are exposed to soot. Within automotive systems the reactivity of exhaust soot will affect the regeneration efficiency of diesel and gasoline particulate filters. For example, Song et al. observed increased concentration of oxygen-containing functional groups on the surface of soot structures leading to an increased efficiency of oxidation and therefore DPF regeneration [25]. Lapuerta et al. observed that while biodiesel soot possessed a more ordered and graphitic (and therefore in theory less reactive) structure than diesel soot, it was more efficiently oxidised in the particulate filter due to smaller primary particles increasing available surface area, and differences in cake formation on the filter [26]. The morphology and reactivity of soot emitted into the ambient environment has also been observed to affect the extent of inhalation and of deposition in lungs [27], contribute to global warming via light extinction and interaction with reactive ambient species [28], and disrupt marine bacterial ecosystems [29].

As the size of soot nanoparticles is typically well below one micrometre, high resolution transmission electron microscopy (HRTEM) is the preferred imaging technique for subsequent nanoscale analysis of morphology and structure. TEM has been used to characterise soot from both the exhaust gas [18–21,24] and lubricating oil [7,17,18,24] of internal combustion engines, as well as soot from diffusion flames [23,30,31]. Depending on the soot origin the methods of sample collection differ significantly. A variety of techniques have been previously employed to obtain soot from exhaust gas of internal combustion engines. Gaddam and Vander Wal [20] sampled soot directly from the exhaust gas on TEM grids. However, high soot concentration in the exhaust gas can oversaturate the grids. To prevent oversaturation and reduce overlapping of agglomerates, the collection time can be reduced [32]. Alternatively, the exhaust gas can be diluted with clean air [19] or an inert gas, e.g. nitrogen [33], enabling longer collection times. Barone et al. [19] as well as Liati et al. [21] diluted the exhaust gas by a factor of 30 and 13.5, respectively, prior to deposition on TEM grids. To image soot-in-oil samples, the soot agglomerates need to be separated from the lubricating oil. Esangbedo et al. [24] diluted oil samples in heptane and transferred small amounts onto TEM grid after ultrasonically bathing. La Rocca et al. [7] separated soot from the used lubricating oil by multiple cycles of centrifugation and replacing the liquid oil-phase with heptane. Despite altering the observed size distribution of the agglomerates, this procedure enabled observation of the primary particle nanostructure. A similar procedure was employed by Uy et al. [18] using hexane as the solvent. Soot generated from diffusion flames, also known as carbon black, can be collected directly from the flame by thermophoresis on TEM grids, as done by Bhowmick et al. [30] and Schenk et al. [31]. Alfè et al. [23] collected soot from the flame on probes in bulk and subsequently transferred onto TEM grids by ultrasonic agitation in methanol.

Commercially generated carbon black is considered to be a more affordable and reproducible substitute for engine soot in studies on engine wear due to the high costs, long run-times and strong dependency on conditions associated with generating genuine engine-soot. Despite some differences in aggregate size and surface chemistry, Clague et al. [34] found that similarities in the nanostructure enabled the surrogacy, at least for diesel soot. Motamen Salehi et al. [35] used carbon black as substitute for diesel soot to assess the effect of engine oil pump wear. Studies by Mabuchi et al. [36] used an analogous approach to investigate the wear of hydrogen-free diamond-like carbon coatings for engine applications. However, Growney et al. [37] found that the capability of carbon black to substitute engine soot is highly dependent on the lubricating oil formulation. Practical investigations by Antusch et al. [17] showed distinctive differences in the direct comparison of engine soot and carbon black in engine wear tests.

In addition to the assessment of HRTEM images for qualitative information, segments of graphitic layers, known as fringes, can be assessed for their geometric parameters, e.g. fringe length, separation and tortuosity. The fringe length is commonly defined as the distance between the end points along the fringe, i.e. the geodesic length. Tortuosity of the fringes can be obtained from the ratio of their geodesic length and the direct end point distance, i.e. Euclidian length. The separation of a fringe pair can be determined by averaging the perpendicular distance between the two fringes along their geodesic lengths. Following initial advances by Vander Wal et al. [38] towards quantitative measurements, Yehliu et al. [39,40] developed an algorithm comprising image processing and geometric analysis of the fringes with improved quality. Using this algorithm, Jaramillo et al. [41] identified the fringe length and tortuosity for soot from a diesel powered industrial forklift to be 1 nm and 1.17 respectively, while fringe separation was not

analysed. For soot sampled directly from a diesel spray flame, Sakai et al. [42] obtained similar values of fringe length, separation and tortuosity as 0.98 nm, 0.42 nm and 1.23, respectively. Gaddam et al. [20] characterised soot from a GDI engine run under various operating conditions. The fringe length was found to be between 0.72 nm and 0.82 nm, while the tortuosity ranged from 1.176 to 1.21. These values differ from the previous measurements of diesel soot, however, the study did not focus on the differences between the two soot types.

Quantitative analysis of the structure of soot and related nano-carbons can be readily obtained by Raman spectroscopy. This optical technique relies on the inelastic scattering of a monochromatic laser beam, with the resultant shift of the incident photon energy corresponding to specific vibrational modes present in the material under examination. As soot principally comprises carbon, structured at the nanoscale, but often highly disordered at the molecular level, the first-order Raman spectrum is dominated by two broad and strongly overlapping bands within the region $900-1800 \text{ cm}^{-1}$, corresponding to the so-called 'D' (a breathing mode of six-atom rings of A_{1g} symmetry, requiring a defect for its activation, found in defective and nanocrystalline graphitic carbons at ~1350 cm^{-1}) and 'G' bands (a carbon-carbon stretching vibration of E_{2g} symmetry ubiquitously present in graphitised nanostructures at ~1580 cm^{-1}). For carbon black, the intensity ratio of these two bands (I_D:I_G) has been directly related to the fringe length of the nanostructure [38,40]. However, this strategy is not necessarily applicable across all studies as the 'D' band is dispersive in nature, with its position and intensity sensitive to the wavelength of the excitation laser [43]. For example, Uy et al. [18] observed that spectra acquired using a 244 nm ultraviolet laser exhibited no defective 'D' peaks and therefore important information could not be extracted. Moreover, it is now widely recognised that the observed bands in the D/G region more likely represent a superposition of up to five different vibrational modes, deconvolution of which permits quantification of the extent of ordered graphitic ('G' mode), disordered graphitic ('D1', 'D2' and 'D4' mode), and amorphous domains ('D3' mode) within the primary particles [43]. It is interesting to note, however, that for highly disordered carbons the 'D2' mode can be indistinguishable from the 'G' mode [44]. Furthermore, no universal approach for the analysis of the Raman spectra of soot has yet to be established, as the method used for determination of the band intensities varies across different studies. While some reports use maximum peak values, i.e. peak height [18,38], others determine the intensity by measuring the broadness of the peak, as defined by the full width at half maximum [43,45]. Moreover, the quality of the obtained spectra is often dependent on the conditions used for preparation of the sample for analysis, as fluorescence, likely due to contamination from PAH and other substances from the lubricating oil and engine wear, can significantly impact the attainable signal to noise ratio in the resultant spectrum. Uy et al. [18] noted the exhibition of fluorescence, particularly for soot-in-oil samples, despite attempts to purify the sample by dilution in heptane and centrifugation. The procedure was first employed by Clague et al. [34] and recently used in studies by La Rocca et al. [7,46]. However, sample dilution and its impact on the quality of the measurements has not been investigated further.

Knowledge of soot particle formation mechanisms and morphology for GTDI engines is still scarce, with the nanostructure of gasoline soot being reported as non-uniform. This study set out to compare soot-in-oil samples from GTDI engines with better characterised soot from diesel engines, and with carbon black. HRTEM imaging was employed for the initial qualitative assessment of the soot morphology. Carbon particles lacking any apparent long range order in the HRTEM images are here presumed to be entirely amorphous. Subsequent quantitative measurements of the soot nanostructure were obtained by means of fringe analysis. Raman spectroscopy was performed on the samples for further characterisation of the nanostructure, i.e. not only of the graphitic fringes but also to identify the extent of disordered graphitic and amorphous regions. In this context, the effect of sample cleaning procedures on the data quality was assessed.

2. Experimental

2.1. Sample collection and preparation

Two GTDI, two diesel, and one flame-generated soot samples were collected for this study. GTDI samples were collected from engine oil drains of two passenger vehicles during routine maintenance services. One was a three cylinder, 1.0L GTDI Ford EcoBoost engine ('1.0L GTDI' in the following) that was used in primarily urban driving conditions for 8488 km with activated start-stop mode. The other engine was a four cylinder 1.4L GTDI engine from a Volkswagen Polo ('1.4L GTDI' in the following) that was primarily operated in extra-urban driving conditions for 20,284 km with automatic cylinder deactivation enabled. For the first diesel soot sample a 550 cc single cylinder variant of a multi cylinder diesel engine was employed as in a previous study [7] ('SC Diesel' in the following). The engine was filled with clean oil and subsequently operated for a total of 30 h on a laboratory test bed under operating conditions representing light duty diesel applications. Upon completion of the test runs, samples were drawn from the oil sump. The second diesel sample was obtained from oil drains of a 2.0L Jaguar four cylinder engine ('2.0L Diesel' in the following) that was run for 12,875 km under light duty operating conditions. The flame generated soot included in this study was commercially available carbon black 'Cabot Monarch 120'.

While no specific preparation is required for soot samples directly obtained from the exhaust gas [24], soot-in-oil samples have to be cleaned to enable accurate Raman spectroscopy and HRTEM analysis. To separate the soot from the lubricating oil, a cleaning methodology following La Rocca et al. [7] was employed. First, the oil sample was distributed between several hermetically sealed 2 mL volume centrifuge tubes. To remove contaminants bonded to the soot particles, the tubes were then placed in an ultrasonic bath at 20 °C for ten minutes. Subsequently, the tubes were placed in an Eppendorf Centrifuge 5418R at 14,000 rpm (relative centrifugal field value of 16,873 g) for 90 min at 25 °C. The centrifugal force exerted on the sample accelerated the soot particles to the bottom of the tube due to their higher density compared to the lubricating oil. Thus, the supernatant oil could be carefully extracted, leaving only soot and a small amount of remaining oil in the tube. Lastly, the extracted liquid phase was replaced by an equal amount of pure n-heptane. This cycle of ultrasonic bathing, centrifugation and heptane replacement was subsequently repeated multiple times. The respective dilution ratio compared to the initial oil sample was recorded and one tube sample was retained for each cycle. While sample preparation by centrifugation alters the agglomerate structure of soot particles, the nanostructure of primary particles remains unaffected as observed by La Rocca et al. [7].

2.2. HRTEM

HRTEM images were acquired using a JEOL 2100F TEM with a Gatan Orius CCD camera, based in the Nanoscale and Microscale Research Centre (nmRC) at the University of Nottingham. An incident electron beam voltage of 200 kV was used with various magnifications up to 600,000×. Energy-dispersive X-ray (EDX)

spectroscopy was performed with an Oxford Instruments X-Max^N 80 T. Small amounts of the different soot-in-oil samples diluted in heptane were transferred onto TEM grids after five rounds of the above described centrifugation cleaning process. The grids consisted of a copper mesh grid coated with a graphene oxide support film. Upon deposition of the solution the heptane evaporated quickly in ambient conditions. Grids were then washed with diethyl ether to further remove oil contamination and thus enable high quality imaging as previously shown by La Rocca et al. [7,46−48].

2.3. Fringe analysis

For this study a semi-automatic approach was chosen to analyse the ordered regions of the nanostructure. The employed methodology was adapted from Yehliu et al. [39] and written in Matlab®. The region of interest (ROI) was selected by the user for every image. Thereby, only graphitic areas were assessed and interfering objects such as overlapping particles, noisy regions or carbon of the TEM grid disregarded. Several images were analysed for every sample to ensure correct representation of the sample and to account for local variations within. A minimum of 1000 fringes was obtained per sample, of which separations for at least 180 fringe pairs were measured. Parameters for the processing steps were selected based on the pixel scale of the image to account for different magnifications. However, the values were adjusted manually to account for variations in brightness due to sample thickness.

Upon completion of the initial image processing, several additional automated steps were performed to qualitatively clean the preliminary fringes. First, fringes near the border were removed as these could have been partially cut off by applying the ROI cropping. Secondly, presumed artefacts in the form of short fringes (<0.4 nm) were removed as well. However, the threshold value for this artefact removal varies in the literature from as small as the size of a single aromatic ring (0.25 nm) as used by Galvez et al. [49], to the crystallite size of 1.5 nm used by Shim et al. [50]. The value of 0.4 nm used in this study was previously suggested by Vander Wal et al. [51] and was also employed in the underpinning methodology for this algorithm by Yehliu et al. [39]. Further, branched fringes were resolved as these originate either from graphitic defects in the sample or from the image processing steps, i.e. artefacts. The two longest branches were considered to constitute the main fringe, while the shortest branch was kept as an independent fringe. Lastly, fringes with a tortuosity greater than 3 were disregarded, as these are most likely not to represent the actual fringe structure, but rather to occur due to errors in the image processing or the branching algorithm, e.g. two adjacent ends close together.

To measure fringe separations, pairs of fringes were manually selected by the user to ensure that only separations of truly adjacent fringes were considered. The average distance between the fringes was measured perpendicular to the geometric axis of the first selected fringe, i.e. its overall orientation. An upper threshold of 0.5 nm was used, as previously employed by Yehliu et al. [40]. Furthermore, separations of less than 0.34 nm were disregarded due to the minimum interlayer spacing limit in graphite.

2.4. Raman spectroscopy

Information on the molecular-level structure of soot and the presence of contaminants was further obtained by Raman spectroscopy using a Horiba LabRAM HR spectrometer at the nmRC at the University of Nottingham. Single-point spectra were acquired using a 532 nm laser (at 0.25 mW power), a 100× objective and a 300 μm confocal hole. The laser power was limited to 0.25 mW as spectra acquired at higher powers resulted in significant down-shifting of the vibrational modes, consistent with sample heating expected when analysing black materials using visible laser excitation with extended acquisition times [52], and in extreme cases resulted in the photothermal degradation of the sample microstructure. To simultaneously scan a range of Raman shifts, a 600 lines mm^{-1} rotatable diffraction grating along a path length of 800 mm was employed. Spectra were acquired using a Synapse CCD detector (1024 pixels) thermoelectrically cooled to −60 °C. The spectral resolution in this configuration is better than 1.7 cm^{-1}. Before spectra collection, the instrument was calibrated using the zero-order line and a standard Si(100) reference band at 520.7 cm^{-1}. In all cases, spectra acquired from different areas of the sample showed only minimal variation, providing strong evidence for the homogeneity of the samples at the length scales appraised (microns).

To evaluate the effect of dilution and centrifugation on the extent of fluorescence observed in the Raman spectra of the soot extracted from 1.0L GTDI oil, samples were prepared by dropcasting the respective n-heptane soot dispersions onto Si wafers and subsequent spectra collected within the range 650−2220 cm^{-1} with an acquisition time of 15 s and 64 accumulations to automatically remove the spikes due to cosmic rays and improve the signal to noise ratio.

To quantitatively investigate the molecular-level structure of the soot, extracted from both 1.0L GTDI and 2.0L Diesel oil, and carbon black, samples were prepared as described above and subsequent spectra collected within the range 650−2220 cm^{-1} with an acquisition time of 60−120 s and 16−64 accumulations. Prior to spectra collection, the soot samples were photobleached for 30 min in an attempt to deplete the small number of residual artefacts given rise to fluorescence. The acquired spectra were baseline corrected using a third order polynomial fit. Band deconvolution using the five-band model as proposed by Sadezky et al. [43], comprising four Lorenzian and one Gaussian peak profiles, was attempted. However, the D2 mode peak consistently relaxed to zero intensity and was thus not included, consistent with previous reports [37]. Numerous fitting models were explored, yet the only fit that resulted in convergence across all three samples, normalised to fitting parameters and analysis conditions, was obtained using mixed symmetric Gaussian-Lorentzian functions for the G and D1 modes and mixed asymmetric Gaussian-Lorentzian functions to fit the D3 and D4 modes.

3. Results and discussion

3.1. HRTEM

Nanoscale images of the carbon black sample (Fig. 1a and b) show a distinctive core-shell structure of the particles. The centres consist of amorphous nuclei that are surrounded by graphitic carbon layers. Agglomerates of multiple particles (Fig. 1c) were imaged clearly with high resolution. In line with the earlier findings of Clague et al. [34], both 2.0L Diesel (Fig. 1d) and SC Diesel (Fig. 1g) exhibit a similar nanostructure. However, some diesel soot particle cores comprise multiple nuclei (Fig. 1e,h). As these nuclei are more abundant during the early stage of soot formation [53], the present particles are likely to originate from this phase. Wan Mahmood et al. [54] conducted simulations on the in-cylinder formation and distribution of soot. The findings suggested it is most likely the soot early in the combustion stroke that predominantly migrates into the lubricating oil via the oil film on the cylinder walls. Despite similar nanostructure, much smaller particles in fractal-like agglomerates can be observed (Fig. 1f,i); however, the size of these has been shown to be affected by the centrifugation cleaning process by La Rocca et al. [7].
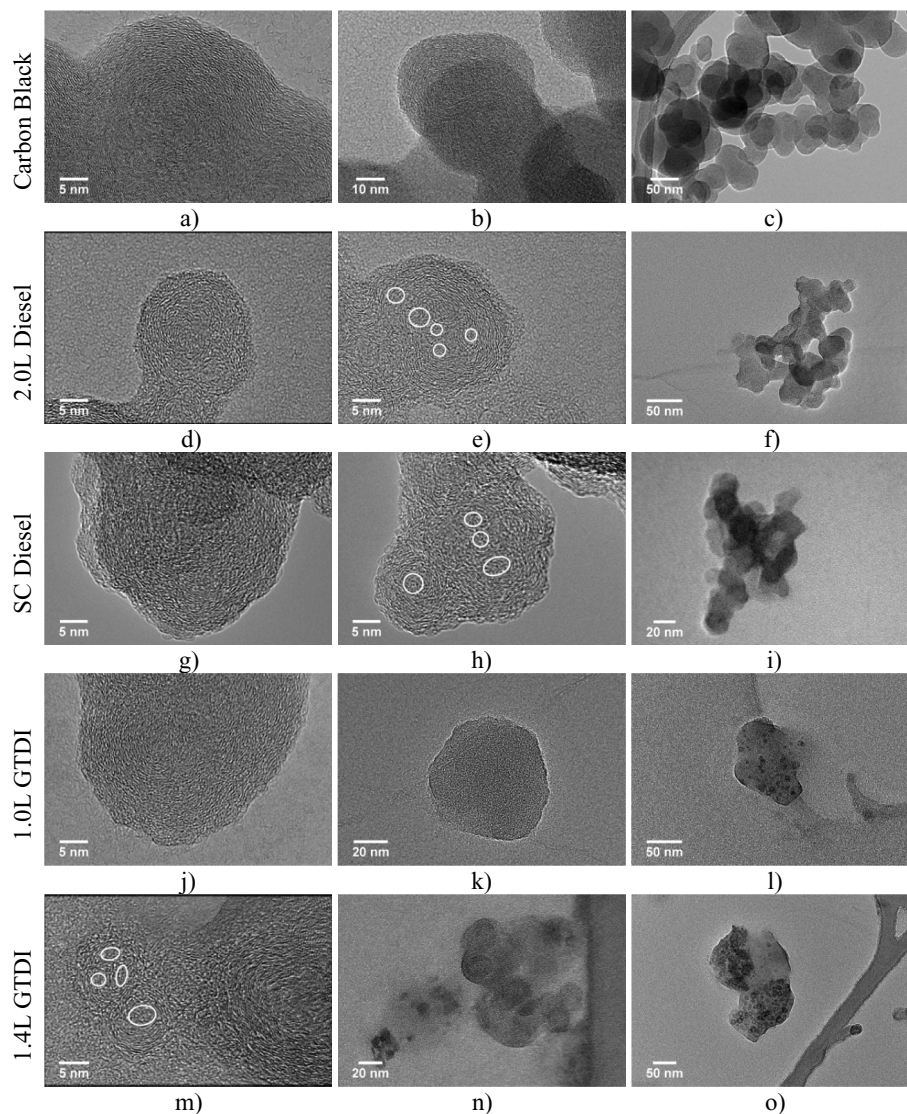
Fig. 1. HRTEM images of carbon black (a–c), 2.0L Diesel (d–f), SC Diesel (g–i), 1.0L GTDI (j–l), and 1.4L GTDI (m–o) soots.

Soot samples from the two GTDI engines appear to have more diverse nanostructures. Some particles exhibited a similar core-shell structure to the diesel soot particles (Fig. 1j,m) including the presence of multiple cores. In contrast to other types of soot, entirely amorphous particles were observed, lacking any apparent long range order (Fig. 1k). Furthermore, the samples contained particles which were previously described as "sludge-like" by Uy et al. [18] (Fig. 1n) and noted to be particularly prone to contamination. However, contrary to their report no decomposition under the electron beam of the TEM was observed here, even after prolonged exposure at 200 kV. Some amorphous particles included small particles with diameters of only a few nanometers embedded within them (Fig. 1l,o). On the nanoscale, these particles exhibited localized crystalline structures (Fig. 2). Similar regions were observed by La Rocca et al. [46] on the surface of regular graphitic primary particles of GDI soot-in-oil. While the surface crystalline regions decomposed under the electron beam, indicating volatiles as their source, the small particles here remained without any sign of decomposition. For diesel soot-in-oil, Sharma et al. [55] also found crystalline regions within particles with EDX spectroscopy measurements pointing towards lubricant oil and engine wear. EDX

spectroscopy measurements of the crystalline regions in amorphous particles (Fig. 3) show traces of various elements (Table 1). Ca, S, and P are commonly associated with additives in the lubricating oil, while Fe, Cr, and O likely stem from the engine wear [18,55,56]. However, Fe and Cr might also be detected due to scattering from the microscope pole piece. F, Na, and Si can originate from multiple sources such as further oil additives or contamination. C and O are associated with the TEM grid and the supporting film respectively, however, the latter can also stem from organic fractions. Despite most of the C stemming from the soot particles, some is attributable to the supporting graphene oxide film.

Crystalline regions embedded within the soot structure were previously found to promote wear and abrasion in engines [57]. Sharma et al. [58] observed such behaviour in diesel engines particularly with increasing engine age. However, here crystalline regions are only observed in the GTDI samples, suggesting a difference between the soot types. The entirely amorphous regions exclusive to the GTDI sample could promote interaction with the lubricating oil. Furthermore, the graphitic nanostructure of regular primary particles could be different. To quantify such differences,
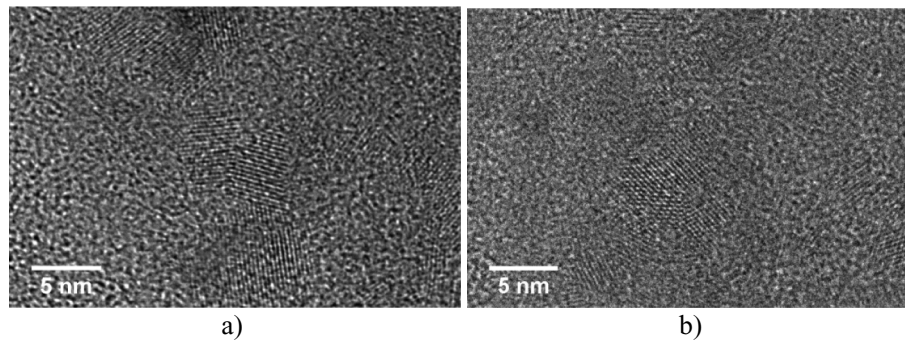
Fig. 2. Enlarged crystallite regions within 1.0L GTDI (a) and 1.4L GTDI (b) soots.
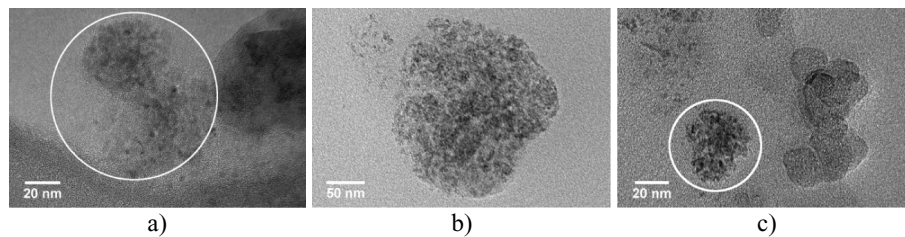
Fig. 3. Amorphous regions with embedded particles and crystallite regions within 1.0L GTDI (a) and 1.4L GTDI (b,c) soots analysed with EDX spectroscopy.

Table 1
EDX spectroscopy measurements of 1.0L GTDI and 1.4L GTDI soot particles.

| Element (At %) | 1.0L GTDI | 1.4L GTDI | |
	Fig. 3a	Fig. 3b	Fig. 3c
C	83.3	84.2	87.1
O	6.9	6.8	6.2
F	4	4.1	2.8
Na	0	0.1	0
Si	1.6	0.9	1
P	0.4	0.3	0.5
S	0.2	0.5	0.2
Ca	3	2.8	1.8
Cr	0.2	0.1	0
Fe	0.2	0.1	0.2
Co	0.2	0.1	0

the nanoscale images have to be assessed by fringe analysis.

3.2. Fringe analysis

Computational analysis of the graphitic nanostructure made differences between the samples apparent (Fig. 4). The carbon black sample exhibited the longest fringes of 1.13 nm. The average fringe length for the 2.0L Diesel and SC Diesel were shorter with 1.08 nm and 1.07 nm respectively. The gap between carbon black and the GTDI samples was found to be larger, with 0.97 nm and 0.99 nm for the fringes of 1.0L GTDI and 1.4L GTDI, respectively. These values differ from previously reported findings. Gaddam and Vander Wal [20] found lamellae of GDI soot ranging from 0.72 nm to 0.82 nm, depending on the operating conditions of the engine. A study by Wu et al. [59] on GDI soot showed that the fringe length also varied with the air-fuel-ratio of the engine, from 0.83 nm to 0.91 nm. For soot obtained from diesel engines, Jaramillo et al. [41] and Sakai et al. [42] reported similar fringe lengths of 0.98 nm and 1 nm respectively. However, in studies by Li et al. [9] and Xu et al. [60] the fringe length of diesel soot was observed to be affected by fuel injection splitting (1.16–1.2 nm) and injection timing

(1.12–1.4 nm), respectively. Overall, the reported fringe length ranges for GDI soot (0.72–0.91 nm) and diesel soot (0.98–1.4 nm) show a clear minimum separation of 0.07 nm. The difference between both soot types was here found to be about 0.1 nm, therewith confirming this observation.

In all of the studies mentioned above, the soot samples were collected either directly or after dilution from the exhaust gas of internal combustion engines run at specific operating conditions. As the soot samples in this study are obtained from the lubricating oil, the soot represents a range of operating conditions. Moreover, primarily early soot migrates into the lubricating oil as mentioned above [54]. Thus, the soot-in-oil would be less oxidised than soot from the exhaust gas due to a shorter residence time in the combustion chamber. Jaramillo et al. [41] found a linear decrease of the fringe length with increasing degree of oxidation of diesel soot. Similarly, Rohani and Bae [61] observed lower fringe length and higher tortuosity for soot obtained directly from the in-cylinder spray than for particles from the exhaust gas. This would explain the numerical difference between the obtained fringe lengths for the samples in this study and the previously reported values.

Regarding carbon black, Jaramillo et al. [41] found the fringe length to be shorter than for diesel soot (0.8–0.9 nm). In contrast, Seong and Boehman [45] found that the crystallite width is higher for carbon black than for engine soots. The latter is supported by measurements in this work. However, different types of carbon black were analysed across the studies. The nanostructure can change significantly with the type of carbon black and sample preparation, as shown by Yehliu et al. for various heat treatments [40]. The present carbon black sample appears to be a particularly ordered/graphitic type.

The fringes of all engine soot samples were found to have nearly the same degree of tortuosity with 1.13 for all but the SC Diesel sample with 1.12 (see Fig. 4b). In contrast, the carbon black sample exhibits the least tortuous graphitic layers with a value of 1.09. Hence, it is assumed that the difference stems from the sample origin, i.e. flame generated vs. internal combustion engines. Again, previously reported numbers differ slightly from the obtained
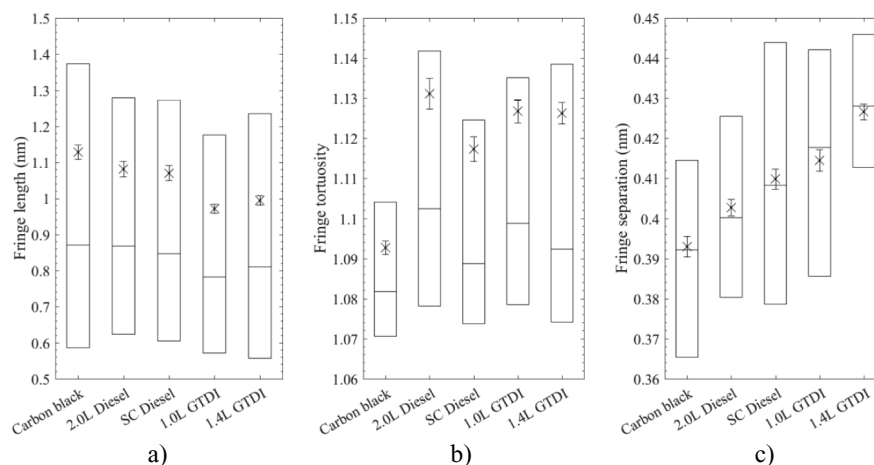
Fig. 4. Comparison of the fringe length (a), the fringe tortuosity (b), and the fringe separation (c) of carbon black, 2.0L Diesel, SC Diesel, 1.0L GTDI and 1.4L GTDI soots obtained by fringe analysis of HRTEM images. The median with interquartile range is indicated by boxes, the markers indicate the mean values with error bars.

measurements. Gaddam and Vander Wal [20] found the tortuosity of GDI soot to be between 1.18 and 1.21 depending on the operating conditions of the engine. Wu et al. [59] observed a tortuosity range of 1.44–1.49 by varying the air-to-fuel ratio of a GDI engine. For diesel engine soot Sakai et al. [42] identified a fringe tortuosity of 1.23 and Jaramillo et al. [41] of 1.17. In a study by Li et al. [9] changes to the diesel fuel injection, i.e. single or multiple injections, lead to a tortuosity range of 1.13–1.2. Furthermore, Xu et al. [60] reported a similar range of 1.12–1.25 for different injection timings and cylinder pressures of a diesel engine. Overall, the reported tortuosities for diesel soot (1.12–1.25) lie within the range of tortuosities for GDI soot (1.18–1.49). Tortuosities observed in this study are at the lower end of these ranges. However, this could be attributed again to the effect of early migration into the lubricating oil and thus a comparitively lower degree of oxidation.

Unlike the two aforementioned parameters, the samples show no kind of grouping. The graphitic layers in carbon black are the closest with average separation of 0.393 nm (see Fig. 4c). The remaining samples show increasingly larger separations: 0.403, 0.410, 0.414 and 0.427 nm for 2.0L Diesel, SC Diesel, 1.0L GTDI and 1.4L GTDI soots, respectively. All engine soots exhibit larger spacings between graphitic layers, with GTDI soot lamellae more apart than those of diesel soot. However, the difference among the samples of the same fuel type is larger than the gap between the two closest GTDI and diesel samples. In a previous study by Wu et al. [59] the fringe separation of GDI soot samples obtained from the exhaust gas ranged 0.38–0.41 nm depending on the air-to-fuel ratio. Sakai et al. [42] found a greater fringe separation of 0.42 nm for the graphitic layers of diesel soot sampled from the in-cylinder spray flame. This could potentially stem from the point of sampling. Soot obtained from the exhaust gas is more oxidised than that formed in the combustion chamber as mentioned above. For carbon black, Yehliu et al. [40] found decreasing fringe separation for more graphitic samples. A more ordered nanostructure reduces the number of defects and thus allows the layers to be stacked more closely. Hence, it is here suggested that the fringe separation decreases with progressing oxidation of soot, as the lamellae in the graphitic structure realign. This assumption is supported by the obtained results.

Overall, the three soot types exhibit distinctive differences in nanostructure. The GTDI soot is the least ordered of the three, followed by the diesel soot samples, and carbon black with the most ordered nanostructure. This can affect both the reactivity and the

oxidation behaviour of the soot [59]. The less ordered the carbon structure, the more graphene layer edge sites are present. Consequently, the soot would be more prone to oxidation and could interact with the lubricating oil to a greater extend [62]. The wear behaviour would be altered and the effectiveness of detergents in the lubricating oil would be impaired [57].

3.3. Raman spectroscopy

To probe the effectiveness of the combined dilution and centrifugation procedures to remove the contaminants from 1.0L GTDI oil giving rise to fluorescence under visible excitation, 532 nm Raman spectra from soot sampled at different extents of purification were analysed (Fig. 5). The pilot study with only four centrifugation cycles (1:2000 oil:heptane dilution ratio) yielded a significant background from fluorescence and thus a spectrum too noisy to be informative. Further centrifugation and increasing the oil:heptane ratio significantly decreased the background fluorescence, most noticeably when increasing the dilution from 1:2000 to 1:75,000, which reduces the background fluorescence at 700 cm^{-1} (553 nm) three-fold from 17,800 to 5900 counts (Fig. 6). Beyond 1:75,000 dilution, the reduction is less pronounced with only a 38% reduction in fluorescence from 5900 to 3650 counts when increasing the dilution to 1:5 $\times$ 10^8. Further purification was not deemed necessary as residual fluorescence could be effectively removed by photobleaching the appraised area of the sample immediately prior to spectra acquisition. Interestingly, the residual fluorescence observed in the Raman spectrum of gasoline soot was approximately ten times higher than that noted for diesel soot under the same dilution ratio and spectral acquisition parameters. This would imply that gasoline soot contains a higher proportion of organic compounds, such as aromatics and PAH, which is supported by the higher PN associated with GTDI engines, a result of increased nucleation during combustion. The observation of high quantities of organic matter, giving rise to fluorescence, in the GTDI sample is supported by the reports of Uy et al. [18] and Gaddam et al. [20], the former of which used an analogous procedure to that reported here in an attempt to remove the contaminants. It is interesting to note, however, that despite the authors utilising more centrifugation steps, high fluorescence continued to be observed, suggesting that the dilution factor (4:1 hexane:oil in Uy et al. [18]; 5 $\times$ 10^8:1 heptane:oil here) was more critical for effective purification.

Raman spectroscopic analysis of carbon black (Fig. 5a) - which
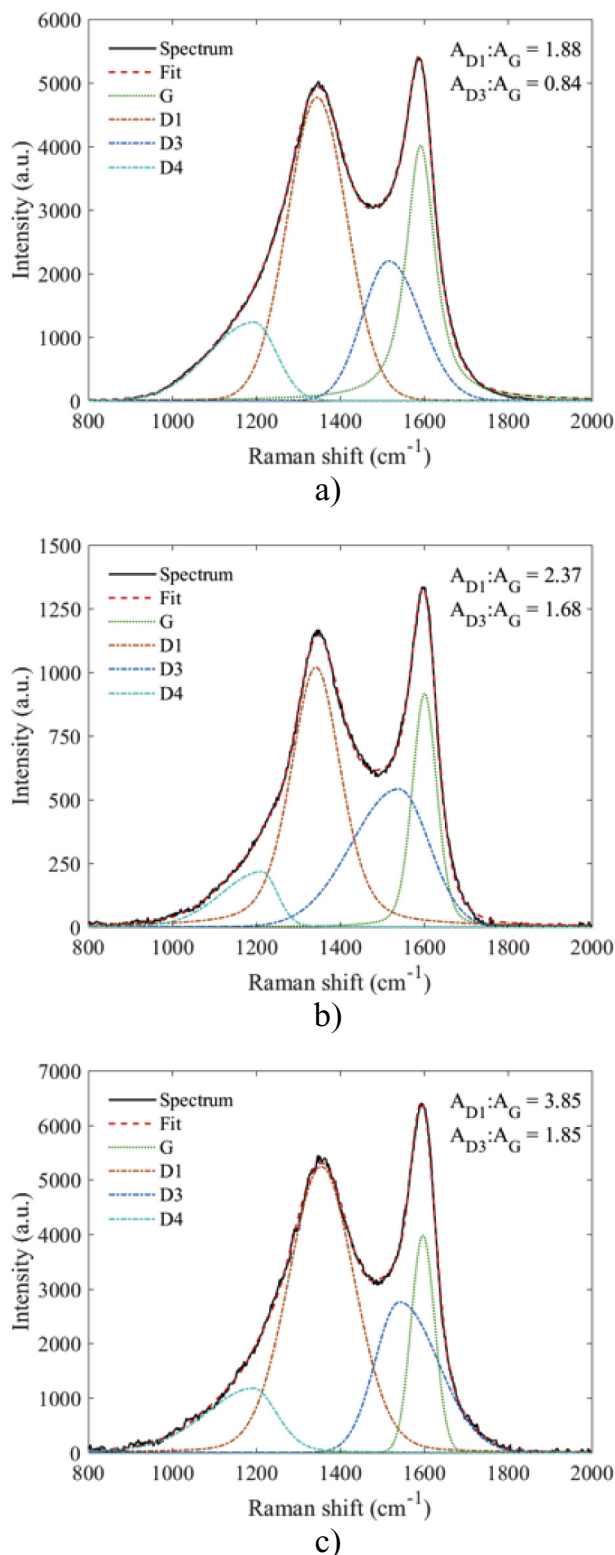
Fig. 5. Baseline corrected Raman spectra with fitted G, D1, D3 and D4 bands Raman spectra of carbon black (a), 2.0L Diesel (b) and 1.0L GTDI (c). The goodness of fit χ^2 is 2.98, 2.97 and 2.97 respectively. (A colour version of this figure can be viewed online.)

required no specific preparation and only minimal baseline subtraction − yielded a spectrum with high signal to noise and effectively no fluorescence as expected for a non-contaminated sample, which was fit using a four-band model (G, D1, D3 and D4 bands). The goodness of fit was $\chi^2 = 2.98$, suggesting effect convergence to a local minimum and therefore an acceptable fit [43]. The baseline-corrected spectra relating to the purified diesel and GTDI soot samples (Fig. 5b and c, respectively) were also fitted with the same four-band model, both achieving $\chi^2 = 2.97$. This goodness of fit matches that obtained for carbon black, highlighting the success of the cleaning procedure for the soot samples. The four-band model utilised in this study represented the best possible fit achievable for these samples; the self-consistency of fitting parameters ensures that the trends observed for the samples explicitly investigated here are meaningful. Furthermore, owing to the improved accuracy and relevance of peak areas (as opposed to peak heights) and the asymmetric nature of the D3 and D4 bands, it was decided that the integrated area under the curve was the most suitable diagnostic for band intensity and thus relative spectral contribution. The ratio of band areas A_{D1} (arising from the graphene layer edge sites suggesting defective graphitic structures) and A_{D3} (arising from amorphous carbon), relative to A_G (arising from graphitic carbon), were the two metrics used to compare the samples. The 0.49 increase seen in $A_{D1}:A_G$ (the ratio of disorder to order within the graphic lattices) between carbon black and diesel soot is related to a decrease in the lamella size (fringe length) and an increase in the disorder (tortuosity) within the sample. While the 0.49 increase represents a 26% increase for diesel over carbon black, the 1.0L GTDI soot shows a 1.97 increase, equivalent to 105%. This value suggests that the 1.0L GTDI soot contains much smaller lamella, a substantial decrease in the basal plane to edge site carbon atoms fraction, and a significant increase in reactivity over both diesel soot and carbon black. In addition, $A_{D3}:A_G$ (the ratio of amorphous to graphitic carbon) was 100% higher for diesel soot relative to carbon black. The relative increase between 1.0L GTDI soot and carbon black is less significant compared to diesel soot showing only a 120% increase. This implies that the high amorphous carbon content is characteristic of engine-produced soot, while more defective carbon is present in the gasoline produced soot.

These observations are in line with the findings of the fringe analysis. Furthermore, the obtained fringe parameters were directly compared with the corresponding $A_{D1}:A_G$ ratios of the respective samples (Fig. 7). A strong linear correlation was found in terms of the fringe length and an inverse correlation for fringe separation, with R^2 values of 0.997 and 0.936 respectively. Thus, the fringe analysis was validated as samples with a greater extend of defective graphitic structures would also exhibit shorter and less densely aligned carbon layers. In contrast, the tortuosity values do not correlate linearly with the $A_{D1}:A_G$ ratios ($R^2 = 0.385$). Instead, it appears that there is a difference in tortuosity between soot from internal combustion engines and carbon black.

4. Conclusions

Two GTDI, two diesel engines, and one carbon black sample were analysed for their nanostructure characteristics:

- HRTEM images show a common core-shell nanostructure among all samples. While the diesel samples only diverge slightly from the highly ordered carbon black, the GTDI samples show a greater diversity in structure types. Entirely amorphous particles were observed, with some exhibiting crystalline
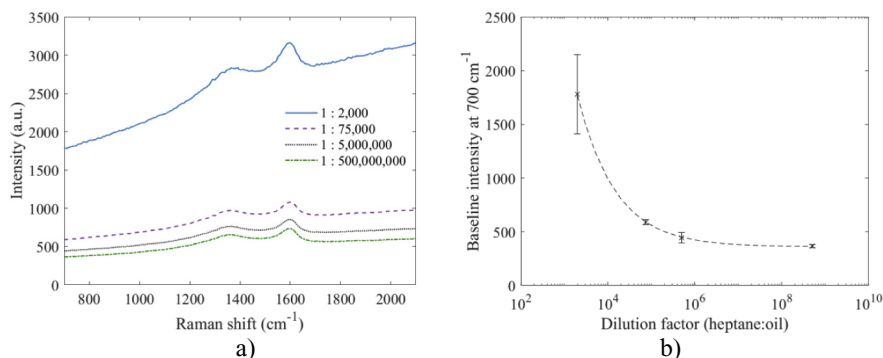
Fig. 6. Effect of heptane dilution on the background intensity of fluorescence in Raman spectra (a) and baseline intensity at 700 cm^{-1} for 1.0L GTDI with dashed trendline (b). (A colour version of this figure can be viewed online.)
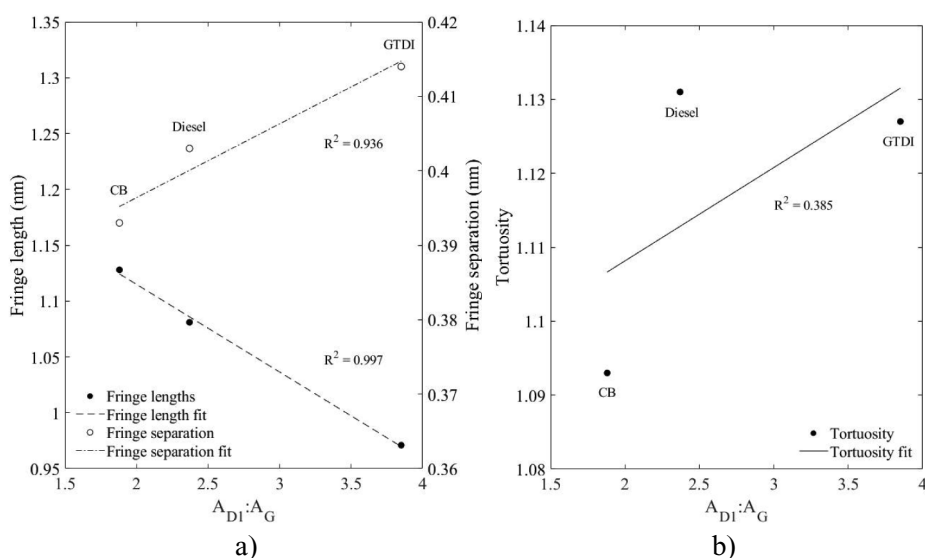
Fig. 7. Correlation of $A_{D1}:A_G$ ratio from Raman spectroscopy with fringe length and separation (a) and with fringe tortuosity (b) from fringe analysis for carbon black (CB), 2.0L Diesel (Diesel), and 1.0L GTDI (GTDI).

regions. Subsequent EDX spectroscopy analysis suggested additives of lubricant oil and wear materials as the source of these embedded phases. In contrast to previous studies, no decomposition under the electron beam was observed.

- Fringe analysis allowed for quantification of differences between particles with similar graphitic nanostructure. The fringe length varied depending on the type of soot, with GTDI soot exhibiting the shortest fringes of 0.97–0.99 nm and longer fringes for diesel soot with 1.07–1.08 nm (+9.7%) as well as carbon black with 1.13 nm (+15.1%). Fringe tortuosity was similar among the engine soot samples with 1.12–1.13, but was lower for carbon black by 3.3% (1.09). Fringe separation showed a continuous trend between samples: carbon black exhibited the closest layers (0.39 nm), diesel soot in the mid range (0.40–0.41 nm), and GTDI soot the largest separation (0.41–0.42 nm).

- Assessment of the sample preparation on the quality of Raman spectra showed a three fold reduction of fluorescence when increasing the dilution ratio from 1:2000 to 1:75,000. However, further increases in dilution ratio above this point did not yield significant reductions of fluorescence.

- Fitting of the obtained Raman spectra with a four-band approach, excluding the contribution from the D2 band, gave acceptable goodness of fit ($\chi^2 < 3$). The $A_{D1}:A_G$ values were 1.88 for carbon black, 2.37 for 2.0L Diesel soot and 3.85 for 1.0L GTDI soot, suggesting 1.0L GTDI soot was the most structurally disordered sample. The $A_{D3}:A_G$ values showed a similar trend with 0.84 for carbon black, 1.68 for 2.0L Diesel soot and 1.85 for 1.0L GTDI soot, indicating the highest fraction of amorphous carbon in 1.0L GTDI soot.

- A strong linear correlation was found between $A_{D1}:A_G$ and the fringe length as well as the fringe separation with R^2 values of 0.997 and 0.936 respectively, validating the fringe analysis. However, fringe tortuosity showed no linear correlation but rather a difference between carbon black and soot from internal combustion engines.

References

[1] F. Zhao, M.C. Lai, D.L. Harrington, Automotive spark-ignited direct-injection gasoline engines, Prog. Energy Combust. Sci. 25 (5) (1999) 437–562, https://doi.org/10.1016/S0360-1285(99)00004-0.

[2] P. Leduc, B. Dubar, A. Ranini, G. Monnier, Downsizing of gasoline engine: an efficient way to reduce CO2 emissions, Oil Gas Sci. Technol. 58 (1) (2003) 115–127, https://doi.org/10.2516/ogst:2003008.

[3] J.W.G. Turner, A. Popplewell, S. Richardson, A.G.J. Lewis, S. Akehurst, C.J. Brace, et al., Ultra boost for economy: realizing a 60% downsized engine concept, in: IMechE (Ed.), Intern. Combust. Engines Performance, Fuel Econ. Emiss., Woodhead Publishing, 2013, pp. 3–17, https://doi.org/10.1533/9781782421849.1.3.

[4] J.B. Heywood, Internal Combustion Engine Fundamentals, McGraw-Hill, New York, 1988.

[5] A short introduction to the problem - structure of the following parts, in: H. Bockhorn (Ed.), Soot Form. Combust. Mech. Model., Springer, Berlin, Heidelberg, 1994, pp. 3–7, https://doi.org/10.1007/978-3-642-85167-4_1.

[6] H. Richter, J.B. Howard, Formation of Polycyclic Aromatic Hydrocarbons and Their Growth to Soot - a Review of Chemical Reaction Pathways, 2000, https://doi.org/10.1016/S0360-1285(00)00009-5.

[7] A. La Rocca, G. Di Liberto, P.J. Shayler, M.W. Fay, The nanostructure of soot-in-oil particles and agglomerates from an automotive diesel engine, Tribol. Int. 61 (2013) 80–87, https://doi.org/10.1016/j.triboint.2012.12.002.

[8] C. Wang, H. Xu, J.M. Herreros, J. Wang, R. Cracknell, Impact of fuel and injection system on particle emissions from a GDI engine, Appl. Energy 132 (2014) 178–191, https://doi.org/10.1016/j.apenergy.2014.06.012.

[9] X. Li, C. Guan, Y. Luo, Z. Huang, Effect of multiple-injection strategies on diesel engine exhaust particle size and nanostructure, J. Aerosol Sci. 89 (2015) 69–76, https://doi.org/10.1016/j.jaerosci.2015.07.008.

[10] X. He, M.A. Ratcliff, B.T. Zigler, Effects of gasoline direct injection engine operating parameters on particle number emissions, Energy Fuels 26 (4) (2012) 2014–2027, https://doi.org/10.1021/ef201917p.

[11] Q. Wang, C. Yao, Z. Dou, B. Wang, T. Wu, Effect of intake pre-heating and injection timing on combustion and emission characteristics of a methanol fumigated diesel engine at part load, Fuel 159 (2015) 796–802, https://doi.org/10.1016/j.fuel.2015.07.032.

[12] M. Saffaripour, T.W. Chan, F. Liu, K.A. Thomson, G.J. Smallwood, J. Kubsh, et al., Effect of drive cycle and gasoline particulate filter on the size and morphology of soot particles emitted from a gasoline-direct-injection vehicle, Environ. Sci. Technol. 49 (19) (2015) 11950–11958, https://doi.org/10.1021/acs.est.5b02185.

[13] F. Bonatesta, E. Chiappetta, A. La Rocca, Part-load particulate matter from a GDI engine and the connection with combustion characteristics, Appl. Energy 124 (2014) 366–376, https://doi.org/10.1016/j.apenergy.2014.03.030.

[14] D.A. Green, R. Lewis, The effects of soot-contaminated engine oil on wear and friction: a review, Proc. Inst. Mech. Eng. Part D J. Automob. Eng. 222 (9) (2008) 1669–1689, https://doi.org/10.1243/09544070JAUTO468.

[15] M. Gautam, M. Durbha, K. Chitoor, M. Jaraiedi, N. Mariwalla, D. Ripple, Contribution of Soot Contaminated Oils to Wear, SAE Tech. Pap. 981406, 1998, https://doi.org/10.4271/981406.

[16] H. Sato, N. Tokuoka, H. Yamamoto, M. Sasaki, Study on Wear Mechanism by Soot Contaminated in Engine Oil (First Report: Relation between Characteristics of Used Oil and Wear), SAE Tech. Pap. 1999-01-3573, 1999, https://doi.org/10.4271/1999-01-3573.

[17] S. Antusch, M. Dienwiebel, E. Nold, P. Albers, U. Spicher, M. Scherge, On the tribochemical action of engine soot, Wear 269 (1–2) (2010) 1–12, https://doi.org/10.1016/j.wear.2010.02.028.

[18] D. Uy, M.A. Ford, D.T. Jayne, A.E. O'Neill, L.P. Haack, J. Hangas, et al., Characterization of gasoline soot and comparison to diesel soot: morphology, chemistry, and wear, Tribol. Int. 80 (2014) 198–209, https://doi.org/10.1016/j.triboint.2014.06.009.

[19] T.L. Barone, J.M.E. Storey, A.D. Youngquist, J.P. Szybist, An analysis of direct-injection spark-ignition (DISI) soot morphology, Atmos. Environ. 49 (2012) 268–274, https://doi.org/10.1016/j.atmosenv.2011.11.047.

[20] C.K. Gaddam, R.L. Vander Wal, Physical and chemical characterization of SIDI engine particulates, Combust. Flame 160 (11) (2013) 2517–2528, https://doi.org/10.1016/j.combustflame.2013.05.025.

[21] A. Liati, D. Schreiber, P. Dimopoulos Eggenschwiler, Y. Arroyo Rojas Dasilva, A.C. Spiteri, Electron microscopic characterization of soot particulate matter emitted by modern direct injection gasoline engines, Combust. Flame 166 (2016) 307–315, https://doi.org/10.1016/j.combustflame.2016.01.031.

[22] R.L. Vander Wal, A.J. Tomasek, Soot oxidation: dependence upon initial nanostructure, Combust. Flame 134 (1–2) (2003) 1–9, https://doi.org/10.1016/S0010-2180(03)00084-1.

[23] M. Alfè, B. Apicella, R. Barbella, J.N. Rouzaud, A. Tregrossi, A. Ciajolo, Structure-property relationship in nanostructures of young and mature soot in premixed flames, Proc. Combust. Inst. 32 (1) (2009) 697–704, https://doi.org/10.1016/j.proci.2008.06.193.

[24] C. Esangbedo, A.L. Boehman, J.M. Perez, Characteristics of diesel engine soot that lead to excessive oil thickening, Tribol. Int. 47 (2012) 194–203, https://doi.org/10.1016/j.triboint.2011.11.003.

[25] J. Song, M. Alam, A.L. Boehman, Impact of alternative fuels on soot properties and DPF regeneration, Combust. Sci. Technol. 179 (9) (2007) 1991–2037, https://doi.org/10.1080/00102200701386099.

[26] M. Lapuerta, F. Oliva, J.R. Agudelo, A.L. Boehman, Effect of fuel on the soot nanostructure and consequences on loading and regeneration of diesel particulate filters, Combust. Flame 159 (2) (2012) 844–853, https://doi.org/10.1016/j.combustflame.2011.09.003.

[27] D.M. Broday, R. Rosenzweig, Deposition of fractal-like soot aggregates in the human respiratory tract, J. Aerosol Sci. 42 (6) (2011) 372–386, https://doi.org/10.1016/j.jaerosci.2011.03.001.

[28] A.F. Khalizov, H. Xue, L. Wang, J. Zheng, R. Zhang, Enhanced light absorption and scattering by carbon soot aerosol internally mixed with sulfuric acid, J. Phys. Chem. A 113 (6) (2009) 1066–1074, https://doi.org/10.1021/jp807531n.

[29] X. Mari, J. Lefèvre, J. Torréton, Y. Bettarel, O. Pringault, E. Rochelle-Newall, et al., Effects of soot deposition on particle dynamics and microbial processes in marine surface waters, Global Biogeochem. Cycles 28 (7) (2014) 662–678, https://doi.org/10.1002/2014GB004878.

[30] H. Bhowmick, S.K. Biswas, Relationship between physical structure and tribology of single soot particles generated by burning ethylene, Tribol. Lett. 44 (2) (2011) 139–149, https://doi.org/10.1007/s11249-011-9831-5.

[31] M. Schenk, S. Lieb, H. Vieker, A. Beyer, A. Gölzhäuser, H. Wang, et al., Morphology of nascent soot in ethylene flames, Proc. Combust. Inst. 35 (2) (2015) 1879–1886, https://doi.org/10.1016/j.proci.2014.05.009.

[32] M. Lapuerta, J. Barba, A.D. Sediako, M.R. Kholghy, M.J. Thomson, Morphological analysis of soot agglomerates from biodiesel surrogates in a coflow burner, J. Aerosol Sci. 111 (2017) 65–74, https://doi.org/10.1016/j.jaerosci.2017.06.004.

[33] Z. Li, C. Song, J. Song, G. Lv, S. Dong, Z. Zhao, Evolution of the nanostructure, fractal dimension and size of in-cylinder soot during diesel combustion process, Combust. Flame 158 (8) (2011) 1624–1630, https://doi.org/10.1016/j.combustflame.2010.12.006.

[34] A.D.H. Clague, J.B. Donnet, T.K. Wang, J.C.M. Peng, A comparison of diesel engine soot with carbon black, Carbon 37 (10) (1999) 1553–1565, https://doi.org/10.1016/S0008-6223(99)00035-4.

[35] F. Motamen Salehi, A. Morina, A. Neville, The effect of soot and diesel contamination on wear and friction of engine oil pump, Tribol. Int. 115 (February) (2017) 285–296, https://doi.org/10.1016/j.triboint.2017.05.041.

[36] Y. Mabuchi, T. Higuchi, D. Yoshimura, M. Murashima, H. Kousaka, N. Umehara, Influence of carbon black in engine oil on wear of H-free diamond-like carbon coatings, Tribol. Int. 73 (2014) 138–147, https://doi.org/10.1016/j.triboint.2014.01.016.

[37] D.J. Growney, O.O. Mykhaylyk, L. Middlemiss, L.A. Fielding, M.J. Derry, N. Aragrag, et al., Is carbon black a suitable model colloidal substrate for diesel soot? Langmuir 31 (38) (2015) 10358–10369, https://doi.org/10.1021/acs.langmuir.5b02017.

[38] R.L. Vander Wal, A.J. Tomasek, K. Street, D.R. Hull, W.K. Thompson, Carbon nanostructure examined by lattice fringe analysis of high-resolution transmission electron microscopy images, Appl. Spectrosc. 58 (2) (2004) 230–237, https://doi.org/10.1366/000370204322842986.

[39] K. Yehliu, R.L. Vander Wal, A.L. Boehman, Development of an HRTEM image analysis method to quantify carbon nanostructure, Combust. Flame 158 (9) (2011) 1837–1851, https://doi.org/10.1016/j.combustflame.2011.01.009.

[40] K. Yehliu, R.L. Vander Wal, A.L. Boehman, A comparison of soot nanostructure obtained using two high resolution transmission electron microscopy image analysis algorithms, Carbon 49 (13) (2011) 4256–4268, https://doi.org/10.1016/j.carbon.2011.06.003.

[41] I.C. Jaramillo, C.K. Gaddam, R.L. Vander Wal, J.S. Lighty, Effect of nanostructure, oxidative pressure and extent of oxidation on model carbon reactivity, Combust. Flame 162 (5) (2015) 1848–1856, https://doi.org/10.1016/j.combustflame.2014.12.006.

[42] M. Sakai, H. Iguma, K. Kondo, T. Aizawa, Nanostructure Analysis of Primary Soot Particles Directly Sampled in Diesel Spray Flame via HRTEM, SAE Tech. Pap. 2012-01-1722, 2012, https://doi.org/10.4271/2012-01-1722.

[43] A. Sadezky, H. Muckenhuber, H. Grothe, R. Niessner, U. Pöschl, Raman microspectroscopy of soot and related carbonaceous materials: spectral analysis and structural information, Carbon 43 (8) (2005) 1731–1742, https://doi.org/10.1016/j.carbon.2005.02.018.

[44] F.A. Ruiz, M. Cadrazco, A.F. López, J. Valdepeñas, J.R. Agudelo, Impact of dual-fuel combustion with n-butanol or hydrous ethanol on the oxidation reactivity and nanostructure of diesel particulate matter, Fuel 161 (2015) 18–25, https://doi.org/10.1016/j.fuel.2015.08.033.

[45] H.J. Seong, A.L. Boehman, Evaluation of Raman parameters using visible Raman microscopy for soot oxidative reactivity, Energy Fuels 27 (3) (2013) 1613–1624, https://doi.org/10.1021/ef301520y.

[46] A. La Rocca, F. Bonatesta, M.W. Fay, F. Campanella, Characterisation of soot in oil from a gasoline direct injection engine using transmission electron microscopy, Tribol. Int. 86 (2015) 77–84, https://doi.org/10.1016/j.triboint.2015.01.025.

[47] A. La Rocca, G. Di Liberto, P.J. Shayler, C.D.J. Parmenter, M.W. Fay, Application of nanoparticle tracking analysis platform for the measurement of soot-in-oil

agglomerates from automotive engines, Tribol. Int. 70 (2014) 142—147, https://doi.org/10.1016/j.triboint.2013.09.018.

[48] A. La Rocca, J. Campbell, M.W. Fay, O. Orhan, Soot-in-Oil 3D volume recon-struction through the use of electron tomography: an introductory study, Tribol. Lett. 61 (1) (2016), https://doi.org/10.1007/s11249-015-0625-z.

[49] A. Galvez, N. Herlin-Boime, C. Reynaud, C. Clinard, J.N. Rouzaud, Carbon nanoparticles from laser pyrolysis, Carbon 40 (15) (2002) 2775—2789, https://doi.org/10.1016/S0008-6223(02)00195-1.

[50] H.-S. Shim, R.H. Hurt, N.Y.C. Yang, A methodology for analysis of 002 lattice fringe images and its application to combustion-derived carbons, Carbon 38 (1) (2000) 29—45, https://doi.org/10.1016/S0008-6223(99)00096-2.

[51] R.L. Vander Wal, Soot Nanostructure: Definition, Quantification and Implica-tions, SAE Tech. Pap. 2005-01-0964, 2005, https://doi.org/10.4271/2005-01-0964.

[52] M. Lapuerta, F. Oliva, J.R. Agudelo, J.P. Stitt, Optimization of Raman spectros-copy parameters for characterizing soot from different diesel fuels, Combust. Sci. Technol. 183 (11) (2011) 1203—1220, https://doi.org/10.1080/00102202.2011.587484.

[53] A. Liati, P. Dimopoulos Eggenschwiler, D. Schreiber, V. Zelenay, M. Ammann, Variations in diesel soot reactivity along the exhaust after-treatment system, based on the morphology and nanostructure of primary soot particles, Combust. Flame 160 (3) (2013) 671—681, https://doi.org/10.1016/j.combustflame.2012.10.024.

[54] W.M.F. Wan Mahmood, A. La Rocca, P.J. Shayler, F. Bonatesta, I. Pegg, Predicted Paths of Soot Particles in the Cylinders of a Direct Injection Diesel Engine, SAE Tech. Pap. 2012-01-0148, 2012, https://doi.org/10.4271/2012-01-0148.

[55] V. Sharma, D. Uy, A. Gangopadhyay, A. O'Neill, W.A. Paxton, A. Sammut, et al., Structure and chemistry of crankcase and exhaust soot extracted from diesel engines, Carbon 103 (2016) 327—338, https://doi.org/10.1016/j.carbon.2016.03.024.

[56] M. Patel, P.B. Aswath, Structure and chemistry of crankcase and cylinder soot and tribofilms on piston rings from a Mack T-12 dynamometer engine test, Tribol. Int. 77 (2014) 111—121, https://doi.org/10.1016/j.triboint.2014.04.004.

[57] M. Patel, P.B. Aswath, Morphology, structure and chemistry of extracted diesel soot: Part II: X-ray absorption near edge structure (XANES) spectroscopy and high resolution transmission electron microscopy, Tribol. Int. 52 (2012) 17—28, https://doi.org/10.1016/j.triboint.2012.02.022.

[58] V. Sharma, S. Bagi, M. Patel, O. Aderniran, P.B. Aswath, Influence of engine age on morphology and chemistry of diesel soot extracted from crankcase oil, Energy Fuels 30 (3) (2016) 2276—2284, https://doi.org/10.1021/acs.energyfuels.5b02512.

[59] Z. Wu, C. Song, G. Lv, S. Pan, H. Li, Morphology, fractal dimension, size and nanostructure of exhaust particles from a spark-ignition direct-injection en-gine operating at different air—fuel ratios, Fuel 185 (2016) (2016) 709—717, https://doi.org/10.1016/j.fuel.2016.08.025.

[60] Z. Xu, X. Li, C. Guan, Z. Huang, Effects of injection timing on exhaust particle size and nanostructure on a diesel engine at different loads, J. Aerosol Sci. 76 (2014) 28—38, https://doi.org/10.1016/j.jaerosci.2014.05.002.

[61] B. Rohani, C. Bae, Morphology and nano-structure of soot in diesel spray and in engine exhaust, Fuel 203 (2017) 47—56, https://doi.org/10.1016/j.fuel.2017.04.093.

[62] K. Al-Qurashi, A.L. Boehman, Impact of exhaust gas recirculation (EGR) on the oxidative reactivity of diesel engine soot, Combust. Flame 155 (4) (2008) 675—695, https://doi.org/10.1016/j.combustflame.2008.06.002.